Supplement of Atmos. Chem. Phys. Discuss., 14, 22045–22116, 2014
http://www.atmos-chem-phys-discuss.net/14/22045/2014/
doi:10.5194/acpd-14-22045-2014-supplement

Atmospheric Chemistry and Physics Discussions

Supplement of

A comprehensive laboratory study on the immersion freezing behavior of illite NX particles: a comparison of seventeen ice nucleation measurement techniques

N. Hiranuma et al.

Correspondence to: N. Hiranuma (seong.moon@kit.edu)

S1. Supplementary methods

This supplementary information provides additional details for the measurement techniques of immersion freezing of illite NX particles with S1.1. suspension techniques and S1.2. dry-dispersed particle measurement techniques (both in alphabetical order as in **Table 1**). The discussions of measurement uncertainties of temperature and n_s for each measurement technique are also provided. We note that the uncertainty in frozen fraction (α) used in calculating n_s may not be adequate, since the sensitivity of $\Delta\alpha$ (an increase or a decrease in frozen fraction) is much higher at high temperatures which unexceptionally coincide with a low fraction of frozen illite NX.

S1.1. Suspension techniques

Bielefeld Ice Nucleation ARraY (BINARY)

The BINARY setup is an optical freezing apparatus that makes use of the change in droplet brightness during freezing for the automated and simultaneous detection of ice nucleation in 36 microliter-sized droplets. The droplets are positioned on a hydrophobic glass slide that rests on top of a Peltier cooling stage (Linkam LTS 120). The 36 droplets are separated from each other by a polydimethylsiloxane (PDMS) spacer in order to prevent a Wegener-Bergeron-Findeisen process. For a particular illite NX concentration (0.1, 0.5, 2, 5 and 10 mg/mL based on the amount of suspended mass of illite NX sample per H_2O volume) at least 3 experiments with 36 drops each were conducted, resulting in a minimum of at least 108 freezing events at each concentration. The droplet temperature was calibrated based on phase transition temperatures of several compounds over the range from 0 to -40 °C and for rates between 0.1 and 10 °C min^{-1}. Details of the setup and its temperature calibration are presented elsewhere (*Budke and Koop*, 2014). In addition to this temperature calibration no further corrections were made to the dataset of observed individual droplet freezing temperatures. However, if any droplet freezing temperatures of a particular concentration were below -25 °C, this concentration was excluded from the analysis. At these temperatures, the derived n_s for different illite NX mass concentrations deviate from each other, indicating

that ice nucleation in these droplets was not induced by illite NX particles, but rather by ice nucleating impurities contained in the water. This lower temperature limit is also in agreement with the observed 25th percentile freezing temperature value of about -26 °C for pure water samples. Additionally, if at a specific temperature less than 1% of the freezing events in a concentration series occur, the corresponding data point was also excluded.

Experimental uncertainties: The spread of experimentally found transition temperatures in the calibration indicates a quartiles-based error of ± 0.3 °C. Assuming 10% errors in the mass concentration, the droplet volume, and the frozen fraction an error of about 20% is associated to the active site density per mass based on Gaussian error calculation. The maximal error is 35%. For the active site density per surface area an additional error has to be included due to the uncertainty in the specific surface area.

Colorado State University Ice Spectrometer (CSU-IS)

An immersion-freezing method was used to obtain INP temperature spectra for NX-illite clay, both when in bulk suspension and for size-selected particles.

For the bulk clay, a 0.5 wt% suspension was made in 10 mM sodium phosphate buffer (at *pH* 8.7 to match the *pH* of the sample and to prevent flocculation, and filtered through a 0.02 µm Anotop syringe filter (Whatman)) and mixed by tumbling end-over-end at 1 cycle s^{-1} for 30 min (Cole-Palmer, Roto-Torque). Measures of INP were made on this suspension and on a series of 20-fold dilutions to 3.1 x 10^{-6} wt% in the same buffer.

Polydisperse NX-illite particles were generated for size selection using the simple flask generator as described in *Tobo et al*. (2014). For collection of size-selected particles, several grams of dust were placed in a 250 mL conical flask, and dust released by blowing nitrogen in at the base base (~2 L min^{-1}) while agitating the flask in an ultrasonic bath. The particle stream was passed through a dilution tank (N_2 flow rate into the tank ~5 L min^{-1}) and then through a ^{210}Po neutralizer before size selection of particles with a mobility diameter of 500 nm in a DMA (TSI Inc., Model 3081; sheath flow: 4.5 L min^{-1}, sample flow: 1.8 L min^{-1}). This stream was then divided, with 0.3 L min^{-1} passed to a condensation particle counter (CPC, TSI Inc., Model 3010) and 1.50 L min^{-1} drawn through a 47 mm diameter in-line aluminum filter holder (Pall) fitted with a 0.2 µm-diameter-pore Nuclepore track-etched polycarbonate membrane (Whatman). Concentration of 500 nm particles was maintained at around 1,500 cc^{-1} and flow was continued until 127 million particles were collected. Filters and dissembled filter holders had been pre-cleaned, separately, by soaking in 10% H_2O_2 for

10 and 60 min, respectively, followed by three rinses in deionized water (18 MΩ and 0.2 µm-diameter-pore filtered). Filters were dried on foil in a particle-free, laminar flow cabinet, as were filter holder components after excess water was removed with a gas duster.

After particle collection, the filter was transferred to a sterile, 50 mL Falcon polypropylene tube (Corning Life Sciences), 5.0 mL of 0.2 µm-pore-diameter-filtered deionized water added (which contained 1-3 INP mL^{-1} at -23 °C), and particles re-suspended by tumbling for 30 min on the rotator. Measures of INP were made on this suspension and on a 20-fold dilution.

To obtain INP temperature spectra, suspensions were first aliquoted into sterile, 96-well polypropylene polymerase chain reaction (PCR) trays (Life Science Products Inc.) in a laminar flow cabinet. For each dilution, 32 aliquots of 60 µL were dispensed. Trays were capped with polystyrene lids (Nunc microwell plates, Thermo Fisher Scientific Inc.) and transferred to CSU-IS.

The IS was constructed using two 96-well aluminum incubation blocks for PCR plates (VWR) placed end-to-end and encased on their sides and base by cold plates (Lytron). A ULT-80 low temperature bath (Thermo Neslab) circulating SYLTHERM XLT heat transfer fluid (Dow Corning Corporation) was used for cooling. PCR plates were placed in the blocks, the device covered with a plexiglass window and the headspace purged with 1.2 L min^{-1} of filtered (HEPA-CAP, Whatman) nitrogen. Temperature was then lowered at 0.33 °C min^{-1}, measured using a thermistor verification probe (Bio-Rad, Hercules, CA, VPT-0300) inserted into a side well. The number of frozen wells were counted at 0.5 or 1 °C degree intervals, and cumulative numbers of INP mL^{-1} suspension estimated using the formula $\ln(f)/V$, where f is the proportion of droplets not frozen and V is the volume of each aliquot (*Vali*, 1971). This was converted to INP g^{-1} illite and thence to INP m^{-2} illite assuming a surface area of 124 m^2 g^{-1} dust. For size-selected particles, mass was calculated assuming particles were spherical and had a density of 2.65 g cm^{-3}.

Experimental uncertainties: The temperature uncertainty in the CSU-IS technique is ± 0.2 °C (a combination of the uncertainty in the probe and the temperature variation across the blocks due to gradients in cooling). Binomial sampling confidence intervals (95%) were derived using as recommended by *Agresti and Coull* (formula number 2, 1998). Their ranges varied according to the proportion of wells frozen. For a single well frozen out of 32 aliquots, the 95% confidence interval ranged from 18% to 540% of the estimated n_s value, while for 31/32 wells frozen it was 53-149% of the n_s value.

Leeds Nucleation by Immersed Particles Instrument (Leeds-NIPI)

Picolitre-NIPI: the experimental approach employed to study freezing by illite NX particles in droplets 10's µm in diameter has been described in detail by *Broadley et al*. (2012). This instrument has been used in a number of studies of hetereogeneus ice nucleation (*Atkinson et al*., 2013; *Murray et al*., 2011; *O'Sullivan et al*., 2014). Briefly, droplets of dust suspension are generated using a nebuliser and allowed to settle onto a hydrophobic coated glass slide. The droplets are sealed in oil and then transferred to a microscope cold stage where they are cooled at a controlled rate. The droplet freezing temperatures are recorded using a camera coupled to the microscope.

Microlitre-NIPI: This more recently developed technique makes use of larger droplets (~1 mm) which thereforecontain a greater surface area of dust for a constant dust concentration. The µl-NIPI is sensitive to smaller values of n_s than the pl-NIPI. This instrument is described by *Atkinson et al*. (2013), *O'Sullivan et al*. (2014) and also used by *Herbert et al*. (2014) for heterogeneous ice nucleation studies. It has not previously been used for illite NX particles. Briefly, experiments involve pippetting 1 µl volume droplets of suspension onto a hydrophobic glass slide positioned on a cold stage. The cold stage is cooled by a stirling engine (Grant-Asymptote EF600) and droplet freezing is recorded using a digital camera.Values of n_s have been extended to much higher temperatures using the µl-NIPI.

The recorded images of droplets freezing for both NIPI experiments are analysed in order to determine the freezing temperature of each droplet. For the pl-NIPI the size of each droplet is also recorded. In the µl-NIPI experiments droplets are of a uniform size since they were pipetted onto the surface.

Experimental uncertainties: To calculate error in n_s the Leeds-NIPI measurement, errors from the BET surface area, the weights used to make up suspensions, dust density and estimated pipetting error to calculate an error in the amount of IN surface area per droplet were propagated. The resulting error for 0.1wt% and 1wt% suspension was ± 18.9% and ± 10.8% in n_s, respectively. The temperature error was calculated by taking the random error of the thermocouple used to measure temperature in a cold stage and propagated this with the melting point range observed for water. This resulted in a maximum error of less than ± 0.4°C.

Mainz Acoustic Levitator (M-AL)

Inside the acoustic levitator (type APOS BA 10 from TEC59) a standing ultrasonic wave is produced by interference where drops can be levitated at the nodes. It is installed inside a walk-in cold chamber where the set-up includes the acoustic levitator, a platinum-resistor thermometer Pt100 to measure the ambient temperature, a digital video camera to determine the drop sizes, and an infra-red thermometer to directly and contact-free measure the temperature of the freezing drops. These measurements require a circular spot of approximately 1 mm in diameter and, therefore, the investigated drops had sizes of 2 ± 0.2 mm in diameter. Because of their rather large volume and missing ventilated heat transfer the levitated drops cool down rather slowly while exchanging heat with the ambient air in the cold chamber. This results in a non-linear cooling rate. During the experiments with illite-NX, the temperature of pure water drops developed as follows (*Diehl et al.,* 2014):

$$T_{drop}(t) = -27.050\ ^{\circ}C + 27.082\ ^{\circ}C \exp\left(-\frac{t}{16.374}\right) \quad \text{(Eqn. S1)}$$

where $T_{drop}(t)$ *is* the drop surface temperature, t the time. Individual drops containing polydisperse illite NX particles were levitated one after another and cooled down according to Eqn. S1. The transition from the liquid to the ice phase was clearly defined by a sudden increase of the drop temperature (because of the release of latent heat) recorded from the infra-red thermometer (*Diehl et al.,* 2014). For each particle concentration, approximately 100 drops were observed until they froze and the freezing temperatures, i.e. the lowest drop temperatures were recorded with a measuring error of ± 0.7K. Afterwards, for temperature steps of 1K the fractions of frozen drops were counted.

Experimental uncertainties: The uncertainties for T and n_s are ± 0.7 ˚C and ± 30%, respectively. The n_s uncertainty includes errors of the frozen fractions of drops, the specific particle surface area, the particle masses per drop, and the drop sizes.

Mainz vertical Wind Tunnel (M-WT)

In the Mainz vertical wind tunnel drops are freely floated at their terminal velocities in an air stream. Thus, ventilation and heat transfer are similar to the situation as in the real atmosphere. The wind speed is uniformly distributed around the entire cross section area up to

the boundary layer at the tunnel walls. This ensures that drops float in a stable fashion in the observation section of the tunnel (*Szakáll et al.,* 2009; *Diehl et al*., 2011). The drop size was determined from the recorded wind speed in the tunnel as it must be equal to the terminal velocity of the drop to keep the drop floating in the observation section. The drop temperature was calculated afterwards from the ambient temperature in the wind tunnel and the dew point with an estimated error of ± 1K. Drop sizes of 680 ± 60 μm in diameter were selected because the onset of freezing was determined by direct observation (*Diehl et al.,* 2014). The experiments were performed at constant ambient temperatures, i.e. the wind tunnel was pre-cooled to certain temperatures in steps of 1K. The adaption time of the drops, i.e. the time after which the drop temperature was equal to the ambient temperature was 4 to 5 s (*Diehl et al.,* 2014). Individual drops containing polydisperse illite NX particles were observed for approximately 30 to 40 s. 50 drops were investigated per temperature interval and particle concentration. Afterwards, the fractions of frozen drops were counted for a total observation time of 30 s.

Experimental uncertainties: The uncertainties for T and n_s are ± 1 ˚C and ± 35%, respectively. Similar to M-AL, the n_s uncertainty of M-WT includes errors of the frozen fractions of drops, the specific particle surface area, the particle masses per drop, and the drop sizes.

North Carolina State cold stage (NC State-CS)

The design of the NC State cold stage-supported droplet freezing assay (NC State-CS for brevity) and data reduction technique is described in detail in *Wright and Petters* (2013) and *Hader et al*. (2014). For the experiments reported here aqueous suspensions ranging from 0.0001 to 1.0% w/w of ultrapure water (18.2 MΩ resistivity) and dry illite NX powder were prepared. Droplet populations of two distinct size ranges were investigated. Picodrops were generated by mixing a 15 μL aliquot of bulk suspension with squalene and emulsifying the hydrocarbon-water mixture using a vortex mixer. The emulsion was poured into an aluminum dish holding a hydrophobic glass slide. This resulted in between ~400 and 800 usable droplets per experiment with a typical diameter D ~ 85 μm. Nanodrops were generated by manually placing drops with a syringe needle tip on a squalene covered glass slide and letting the drops settle to the squalene glass interface. This resulted in ~ 80 droplets per experiment with typical diameter D ~660 μm. For all experiments the aluminum dish was cooled at a constant rate of 1ºC min^{-1} and the fraction of unfrozen drops was recorded using a microscope in

increments of dT = 0.17ºC resolution. To account for slightly higher temperatures of the squalene relative to the glass slide, a temperature calibration was applied to the nanodrop data (*Hader et al*., 2014). The resulting fraction of droplets frozen versus temperature data were inverted to find the concentration of INPs using the method of *Vali* (1971):

$$c_{IN}(T) = \frac{ln(f_{unfrozen})}{V_{drop}} \quad \text{(Eqn. S2)}$$

where $c_{IN}(T)$ is the concentration of INP per unit volume water (m^{-3} water), $f_{unfrozen}$ is the fraction of unfrozen drops at each particular temperature, and V_{drop} is the median drop volume of the population. To minimize sample heterogeneity only droplets with 78 μm < D < 102 μm were included in the calculation for picodrops. No restriction was applied to the nanodrops. Furthermore, the warmest two percent of data was removed after the calculation of $c_{IN}(T)$ before plotting due to large uncertainty stemming from poor counting statistics (*Hader et al*., 2014). The nuclei content of the ultrapure water was measured in the above manner, resulting in $c_{impurties}(T)$. A best fit line was determined between -20ºC and -35ºC (approximately a homogeneous freezing point for the size of drops used). No impurities were detected at T > -20ºC. The effective INP content was determined by subtracting the nuclei content in the water, $c_{impurities}(T)$, from the measured $c_{IN}(T)$ in the illite NX suspensions. For most conditions $c_{impurties}(T)$ was negligible relative to $c_{IN}(T)$. The ice nucleation surface active site density was then calculated via

$$n_{s,BET} = \frac{c_{IN}(T) - c_{impurities}(T)}{\rho_w w \theta_{N_2}} \quad \text{(Eqn. S3)}$$

where ρ_w is the density of water (997.1 kg H_2O/m^3 H_2O), w is the mass ratio of dust and water (g dust/g water), θ_{N2} is the N_2-based SSA obtained by BET analysis (124.4 m^2 g^{-1} dust) and $n_{s,BET}$ is the BET-normalized IN active surface-site density (m^{-2} dust).

Experimental uncertainties: The accuracy of the thermistor embedded in the lower aluminum block designed for the -40 < T < 0 °C and digitized with precision ±0.01°C. Repeatability of the temperature where 50% of pure water pico drops froze via homogeneous nucleation was -35.7 °C ± 0.1 °C (n = 5, average diameter of drops ~86 μm). In comparison, *Langham and Mason* (1958) report a median freezing temperature of drops ~ -34.4 °C for this size range. The spread in $n_s(T)$ reported as $\Delta n_s(T)$ = [$n_{s,max}(T) - n_{s,min}(T)/n_{s,average}(T)$ was Δn_s(-30°) = 0.6 (n=4), Δn_s(-25°) = 1.75 (n=4), Δn_s(-23°) = 1.28 (n=3), Δn_s(-20°) = 0.59 (n=2)

University of Colorado Raman microscope cold stage (CU-RMCS)

CU-RMCS has been described previously in detail (*Baustian et al*., 2010; *Schill and Tolbert*, 2013). Briefly, a Nicolet Almega XR Raman spectrometer has been coupled to a research grade Olympus BX-51 microscope with 10x, 20x, 50x, and 100x magnification objectives. This Raman microscope has been outfitted with a Linkam THMS600 environmental cell. Temperature of a cold stage inside the cell is controlled by a Linkam TMS94 automated temperature controller with an accuracy of 0.1 K. Water partial pressure inside the cell is controlled by mixing dry and humidified flows of N_2 and measured by a Buck Research CR-A1 dew point hygrometer in line with the cell. In the present experiments, however, droplets are isolated from the cell humidity by a layer of silicon oil.

To generate droplets for an immersion freezing experiment, a known wt% solution of illite NX sample was aspirated into a Meinhard TR-30 glass concentric nebulizer. The concentration of clay in suspensions was determined gravimetrically. Illite NX powder was used as provided without any previous size selection or modification. Clay solutions were mixed for at least 12 h with a magnetic stir bar prior to use in ice nucleation experiments. To mitigate gravimetric settling prior to nebulization, humidified nitrogen was vigorously bubbled through the clay solutions immediately before aspiration. Humidified N_2 was used as the carrier gas to prevent excess evaporation at the nebulizer nozzle. The nebulized spray was directed at a hydrophobically treated fused-silica disc, and the nebulized droplets were allowed to coagulate into supermicron droplets. After nebulization, a drop of silicon oil was placed over the supermicron droplets, and the entire disk was transferred to the environmental cell. Despite low relative humidities inside the cell, droplets inside the drop of silicon oil did not visibly grow or shrink, even after sitting for 12 hours. Prior to each experiment, droplets were examined under 50x magnification to ensure that suspended material was visually evenly distributed between droplets. Thus, the concentration of clay in the droplets was assumed to be the same as the concentration of clay in the bulk solution. Experiments were video recorded under 10x or 20x magnification at 30 frames per second and freezing events were identified by the sudden appearance of structure within droplets. Ice nucleation frozen fractions were calculated as a function of temperature. Depending on the size of the droplets, frozen fraction curves were separated into four different size bins: 10-20 µm, 20-60 µm, 60-120 µm, and 120-200 µm (lateral diameter). These size bins span droplet volumes from ~0.3 pL to 2.5 nL. In the present experiment, the droplets were cooled from approximately 5 °C to -40 °C at a rate of 10 K min^{-1}. Errors in n_s values are based on the range of surface areas

267 available in each experiment. The temperature error for all droplets, 0.5 K, were determined
268 by repeated homogeneous freezing experiments on ultra-pure water.
269 **Experimental uncertainties:** For CU-RMCS, the errors (%) in log-scaled $n_{s,BET}$
270 $(= 100 \times \frac{log(n_{s,BET}^{measred}) - log(n_{s,BET}^{error})}{log(n_{s,BET}^{measred})})$ derived from surface area deviations were estimated as
271 4.3%.

S1.2. Dry-dispersed particle measurement techniques

Aerosol Interaction and Dynamics in the Atmosphere (AIDA) cloud simulation chamber

Immersion freezing activity of dry illite NX particles pulverized by a rotating brush generator (PALAS, RBG1000) was investigated using AIDA-CECC. A series of expansion experiments with elevated temperature was performed in the temperature range between -27 ˚C and -35 ˚C. The results of a total of eighteen expansion experiments with ten polydisperse and eight size-selected size distributions (200, 300 and 500 nm diameter) are reported in the present study.

AIDA-CECC consists of an 84 m^3 aluminum cylindrical vessel housed in a thermally insulated room. A mechanical pumping system is mounted directly under the AIDA vessel and used for expansion cooling, which actuates cooling during steady pressure drop from 1000 mb to 800 mb (*Möhler et al*., 2003). During the expansion cooling experiment controlled by a mechanical pump, the cooling rates of gas temperature in the vessel typically decrease from ~5 ˚C min^{-1} to <0.1 ˚C min^{-1}. The conditions in the vessel, such as temperature and relative humidity, were continuously homogenized by a mixing ventilator installed on the base of the vessel. The chamber conditions were also monitored by temperature sensors (*Möhler et al*., 2003) and tunable diode laser (TDL) water vapor absorption measurement (*Fahey et al*., 2014) prior to and while running each experiment. The use of AIDA for both immersion mode and deposition mode freezing experiment is described in detail in previous reports (e.g., *Hiranuma et al.,* 2014a and 2014b, respectively) so only a brief description is provided here.

For the immersion mode experiment, spontaneous formation of water droplet occurs at water saturation while continuously cooling. Thereafter, water supersaturation condition in the vessel was maintained by controlled mechanical expansion. At droplet activation, most of clay mineral particles were presumably immersed in water drops leading to droplet-freezing at a characteristic temperature (*Hiranuma et al*., 2014b). Thus, within our definition of singular freezing, immersion ice nucleation activity of clay minerals solely depended on temperature.

Temporal evolution of size distribution and associated particle phase was measured using the welas optical spectrometers (PALAS, Sensor series 2300 and 2500; *Benz et al*., 2005) and a light scattering instrument, *Streulicht-intensitätsmessungen zum optischen*

304 *Nachweis von Eispartikeln*, (SIMONE in *German*; *Schnaiter et al*., 2012) that are directly
305 mounted to the wall of the AIDA vessel. Two independent sensors of a welas deployed on the
306 bottom vessel of AIDA in side by side position were used together to measure ice crystal size
307 distributions over the size range of 0.5 to 150 μm optical diameter every 5 s. Assuming
308 spherical shape of particles, the optical diameter is equivalent to a volume equivalent
309 geometric diameter. The droplet-ice threshold diameter, D_{thresh}, is determined by SIMONE
310 depolarization measurements (*Schnaiter et al*., 2012). The total ice number was calculated by
311 summing ice numbers above the observed D_{thresh}, typically ~30 μm diameter. For the
312 immersion experiments, we typically observe a full activation of droplets (i.e. number of
313 droplets, $N_{droplet}$ > number of aerosols, N_{ae}), but in case of incomplete droplet activation (i.e.
314 $N_{droplet} < N_{ae}$), the total geometric surface is normalized to a droplet number measured by a
315 welas-OPC.

316 **Experimental uncertainties:** Temperature and humidity uncertainty is ± 0.3 ˚C and ±
317 5%, respectively (*Möhler et al*., 2003; *Fahey* et al. ,2014). The uncertainty involved in the n_s
318 estimation for immersion freezing in AIDA-CECC was previously estimated as 35% (*Steinke*
319 *et al*., 2011).
320

321 **CSU Continuous Flow Diffusion Chamber (CSU-CFDC)**
322

323 CSU-CFDC operating principles are described in the earlier works of *Rogers* (1988),
324 *Rogers et al.* (2001) and *Eidhammer et al.* (2010). The current versions of CSU-CFDC used in
325 ground based (CFDC-1F) and aircraft studies (CFDC-1H) are geometrically identical and
326 composed of cylindrical walls that are coated with ice via flooding and expelling water from
327 the chamber when the walls are set at a controlled temperature of ~-27°C before each
328 experimental period. The plate separation is 1.12 cm prior to ice application, which has a
329 typical thickness of 0.015 cm. The chamber is divided into two sections vertically, separated
330 by a Delrin collar. A temperature gradient between the colder (inner) and warmer (outer) ice
331 walls in the upper 50 cm section creates an ice supersaturated field into which an aerosol
332 lamina is directed. The Delrin inlet manifold has a stainless steel knife edge ring threaded into
333 it, so that aerosol flow is directed centrally between two sheath flows of clean and dry air. The
334 ratio of aerosol and sheath flows can be varied, but typically the aerosol lamina represents
335 15% of the 10 L min^{-1} total flow. Ice crystals forming on ice nuclei in the growth region of the
336 chamber enter the lower 30 cm “evaporation” section of the chamber where the two walls are

held equivalently to the original low (inner) wall temperature. When the temperature gradient in the growth section is adjusted to create water supersaturated conditions that activate cloud droplets, these will evaporate to haze sizes in the evaporation section, at least up to some RH_w where they survive, referred to by many as the droplet breakthrough RH_w. Until that high RH_w, only ice crystals and haze particles will exit the CFDC. Upstream of the CFDC, aerosol particle concentrations are measured by a CPC, sometimes after size selection with a DMA. Small numbers of large aerosol particles are removed just in advance of the CFDC inlet manifold using dual single-jet impactors typically set to cutpoint sizes between 1.5 and 2.4 μm depending on the nature of the experiment. Ice crystals and aerosols exiting the CFDC at sizes above approximately 500 nm are counted with an OPC, where the two populations are readily distinguished in different size modes. For the data collected in this work, we counted all particles in size bins above 3 μm as ice particles.

Present CFDC-1F measurements were focused into 5-10 min periods of sampling alternating with periods in which the aerosol sample was filtered in order to determine background frost influences on ice particle counts in the OPC, as described in a number of prior publications. Background counts were quite low, and so were subtracted as a simple average of filter periods before and after sampling.

Polydisperse illite NX particles were generated for size selection using the simple flask generator as described in *Tobo et al*. (2014). For collection of size-selected particles, several grams of dust were placed in a 250 mL conical flask, and dust released by blowing nitrogen in at the base (~2 L min^{-1}) while agitating the flask in an ultrasonic bath. The particle stream was passed through a dilution tank (N_2 flow rate into the tank ~5 L min^{-1}) and then through a ^{210}Po neutralizer before size selection of particles with a mobility diameter of 500 nm in a DMA (TSI Inc., Model 3081; sheath flow: 4.5 L min^{-1}, sample flow: 1.8 L min^{-1}). This stream was then divided, with 0.3 L min^{-1} passed to a CPC (TSI Inc., Model 3010) and 1.50 L min^{-1} drawn by the CFDC. The activated fraction was calculated by taking the ratio of the ice crystal number concentration to the total particle number concentration measured with the CPC.

For comparison with other IN instruments measuring in the immersion mode, we follow *Sullivan et al*. (2010a and 2010b) and a number of other papers from the CSU group in processing aerosol at $RH_w \approx 105$ %, with the understanding that higher active fractions of mineral dusts have been noted in processing up to about 110% RH_w (*Petters et al*., 2009; *DeMott et al*., 2011). We did not raise RH_w to these higher levels in these studies so that we could avoid any influence of droplet breakthrough. We do now report that for representative

atmospheric mineral dusts, activation at 105% RH_w likely underestimates the active fraction measured at 109% RH_w by the CFDC by a factor of 3 across a broad temperature range (*DeMott et al*. 2014).

Particle losses in upstream tubing, the aerosol impactor, and the inlet manifold of the CFDC have been previously estimated as 30% of total condensation nuclei when sampling ambient air (*Rogers et al*. 2001), but only 10% for aerosols in the 100 to 800 nm size range based on laboratory tests (*Prenni et al*. 2009). We did not correct for such losses in the ice nuclei data for 500 nm particles reported for the CFDC.

Experimental uncertainties: The thermodynamic conditions in the CFDC are inferred based on measurements of chamber pressure, wall temperatures and flow rates. Results are reported for the calculated average aerosol lamina position. The solution for the lamina position, and thus its temperature and supersaturation, requires numerical solution (*Rogers*, 1988), thus making the calculation of uncertainty in the conditions more complex than propagation of error. *Richardson* (2009) used Monte-Carlo methods to estimate the uncertainty in reported lamina temperature and supersaturation, assuming the typical 1 °C temperature variation along the length of the CFDC cylindrical walls. On this basis, temperature uncertainty is ±0.5 °C at the reported CFDC processing temperature, independent of processing temperature. Supersaturation uncertainty was found by *Richardson* (2009) to depend inversely on temperature. This uncertainty may be approximated by the relation ΔRH_w (%) = 21.8 - 0.08 T (in Kelvin). Thus, ΔRH_w uncertainty is ±1.6, 2 and 2.4 % at -20, -25, and -30°C, respectively. This temperature uncertainty propagates into and n_s uncertainty of ±60% at any temperature. This dominates over the variation in N_{ice} at any temperature when N_{ice} is determined for statistically meaningful sample periods, as reported.

ElectroDynamic Balance (EDB) levitator

The EDB setup was used for investigation of the contact and immersion freezing of levitated supercooled water droplets colliding with the illite particles. The setup used for the contact freezing experiments is described in detail by (*Hoffmann et al*., 2013a and 2013b) and therefore only briefly explained here. The centerpiece of the setup is an electrodynamic balance (EDB) for levitating charged water microdroplets. The droplets with diameter of 90 µm are produced by a piezoelectric injector (GeSIM model A010-006 SPIP, cylindrical housing) and charged via induction to the value of 1 pC (*Rzesanke et al*., 2012). The aerosol is

generated by a fluidized bed generator operated with synthetic air followed by a multistage impactor to eliminate the super micron particles from the aerosol flow. Specifically, the multi-orifice rotating stage cascade impactor (LPI-ROT 25/0018, HAUKE) operated with five impactor stages (largest cut-off diameter 2 µm) was used as described in *Hoffmann et al.* (2013b). Only particles of the desired electrical mobility diameter (750nm, 550nm and 320nm, as preselected by Differential Mobility Analyzer, TSI Inc., Model 3081) were allowed to enter EDB. After EDB, the particle number concentration was counted by an Ultrafine Condensation Particle Counter (UCPC, TSI Inc., Model 3776).

To perform immersion freezing experiments we have modified the setup in the following way. The supercooled water droplet was exposed to the flow of the aerosol particles only for a limited time t_1. During this time the droplet, if not frozen via contact nucleation mechanism, has collected average number of particles equal to the product of collision rate (calculated theoretically) and the time t_1. After that, the aerosol particles were removed from the flow by switching on the electrostatic precipitator installed just in front of EDB. For $t > t_1$ the droplet can only freeze via the immersion freezing pathway induced by the particles it has already collected during $t < t_1$.

To compare contact and immersion freezing results we calculate the ice nucleating active site (INAS) density n_s, which is given by the following equations:

$$t < t_1\ (contact\ mode):\ \ n_s = -\frac{\ln(1-f_{ice})}{S_{IN} \cdot n_c \cdot t} = \frac{e_c}{S_{IN}} \qquad \text{(Eqn. S4)}$$

$$t > t_1\ (immersion\ mode):\ \ n_s = -\frac{\ln(1-f_{ice}^*)}{S_{IN} \cdot n_c \cdot t_1 \cdot t} \qquad \text{(Eqn. S5)}$$

where f_{ice} is the frozen fraction after time t, e_c is the probability of freezing on a single contact, n_c is a collision rate, S_{IN} is surface area of a single ice nucleating particle, f_{ice}^* is a fraction of droplets frozen heterogeneously after the aerosol flow was switched off.

Experimental uncertainties: The temperature uncertainty is $T \pm 0.2$°C, and the uncertainty of the freezing probability is $e_c \pm 35\%$. The uncertainty for n_s depends on the uncertainty of the BET surface. Assuming a BET uncertainty of 10-20%, the uncertainty is n_s ± 50-69%.

Fast Ice Nucleus CHamber (FINCH)

FINCH is an online instrument in which aerosol particles are activated to ice crystals under different freezing temperatures and supersaturations. It consists of a chamber (stainless steel tube, 80 cm in length, 8.6 cm inner diameter) for which the wall can be cooled down to temperatures between 0 and -65°C. Inside the chamber a specific supersaturation and temperature is reached by mixing the sample flow of ambient aerosol with a warm moist and a cold dry airflow (*Bundke et al*., 2008). By changing the flow rates and/or temperatures of the individual airflows the chamber supersaturation and freezing temperature can be varied relatively quickly. Ice nucleating particles entering the chamber are activated and grow to sizes of a few micrometers. At the end of the growth tube they are counted in an optical particle counter (OPC) similar to the detector described in *Bundke et al*. (2010) (405 nm wavelength laser with a power of 100 mW). It is able to distinguish between water droplets and ice crystals by analyzing the polarization ratio of the scattered circular polarized light (P44/P11 ratio of the scattering matrix; *Hu et al*., 2003) and detects the auto-fluorescence following from excitation of the grown particles with UV light, which is an indication for biological particle material.

The presented FINCH illite NX dataset was obtained during a joint campaign with LACIS at the Leibniz Institute for Tropospheric Research (TROPOS) facility. Therefore the aerosol generation is identical as described for the LACIS experiments (see below). Size-selected illite NX particles of 500 nm in diameter were fed into FINCH, which was operated at a saturation ratio above water saturation and at temperatures between -21 and -28°C. The frozen fraction, α, was calculated by division of the N_{ice} detected by FINCH at a certain freezing temperature and the number concentration of all particles, which was measured in parallel to FINCH by a CPC (TSI Inc., Model 3010).

Experimental uncertainties: The FINCH uncertainties for the freezing temperature are in the range of ± 1.5°C and ± 30% for n_s. A potential systematic over-estimation of the freezing temperature due to imperfect mixing of the individual airflows are a matter of current investigations.

FRankfurt Ice Deposition freezinG Experiment (FRIDGE) diffusion cell

FRIDGE is an isothermal static vacuum vapor diffusion chamber that nucleates ice either on dry particles deposited on a substrate or freezes droplets with immersed particles on a cold stage.

Dry particle measurements: INPs were collected from the dry illite NX particles in AIDA by electrostatic precipitation of the particles onto silicon wafers of 45 mm diameter. After sampling the wafers were placed on the cold table in the FRIDGE isothermal chamber (~500 mL volume; *Klein et al*., 2010), which was then evacuated. Upon inflation of water vapor into the chamber ice crystals grew on the INP, were photographed by a CCD camera, and were counted automatically for around 100 s. It is assumed that one ice crystal represents one INP active at the selected temperature and vapor pressure. Crystals can be evaporated by evacuation of the chamber, and the measurement can be repeated at another temperature and/or supersaturation. The cold stage temperature can be regulated from 0°C to -35°C.

Measurements of immersed particles: Aerosol was generated by dry dispersion of illite NX particles in air and diluted further with purified air. The particle number size distribution of this aerosol in the 0.3-10 µm diameter range was measured by a TSI 3330-OPS. Illite NX particles were collected by filtration of the aerosol using cellulose nitrate membrane filters (Millipore, HABP04700). After sampling the filters were placed in vials with 10 mL of deionized water. Particles were extracted from the filters by agitating for 10 min in an ultrasonic bath. About 80 droplets of 0.5 µl volume each were taken from the washing solution with an Eppendorff-pipette and were placed randomly on a silicon wafer on the cold stage. The temperature of the cold stage was lowered by 1°C min^{-1} and the number of drops that froze at each temperature was recorded by the CCD camera and counted. This process was repeated several times with fresh droplets. The actual number concentration of INP derived from this measurement builds on the drop freezing concept of *Vali* (1971) as modified by *Ardon-Dryer and Levin* (2014), and is given by

$$K'(T) = \frac{1}{V} \times [\ln(N_0) - \ln(N(T))] \times \frac{x}{y} \qquad \text{(Eqn. S6)}$$

where $K'(T)$ is the cumulative INP concentration at a temperature T. The droplet volume is given by V, N_0 is the total number of droplets, $N(T)$ is the number of frozen droplets at

temperature, T. The variable x is the volume of water used to wash the particles from the filter and y the volume of air sampled through the filter.

Experimental uncertainties: FRIDGE measurement uncertainties are $T \pm 0.2$°C and $n_s \pm 40\%$ at -20°C. The n_s error may become lower with decreasing temperature.

Leipzig Aerosol Cloud Interaction Simulator (LACIS)

LACIS was used in its immersion freezing mode (*Hartmann et al*., 2011) to study immersion freezing efficiency of illite NX particles. LACIS measurements were performed on size segregated particles. Particle generation was done using a similar set-up as e.g. described in *Wex et al*. (2014). In short, illite NX particles were made airborne using a fluidized bed. Subsequently, particles larger than those which should be examined were removed from the aerosol using a micro orifice uniform deposition impactor (MOUDI, MSP Corporation, USA, Model 100R) and a cyclone. Downstream, a neutralizer established a bipolar equilibrium charge distribution on the particles. Then particles were size-selected by a DMA (Type Vienna Hauke medium; aerosol to sheath air flow ratio of 1:10), and selected particle sizes were 300nm, 500nm and 700nm. The aerosol was then provided for further analysis.

The before mentioned removal of larger particles was done to minimize the number of multiply charged particles that pass the DMA, and measurements with a UHSAS (Ultra-High Sensitivity Aerosol Spectrometer, DMT) behind the DMA were done to confirm that the number of multiply charged particles could be neglected.

Size-selected aerosol particles were also fed into a CPC (TSI Inc., Model 3010), and into LACIS. LACIS is a flow tube, consisting of 7 sections where each is 1m long. Each section can be temperature controlled separately. Temperatures can go down to -40°C. Before entering the flow tube, by use of a humidifier (Perma Pure, PH-30T-24KS), the sheath air stream is hydrated such that droplets form on the aerosol particles upon cooling, i.e. while passing through the flow tube. The droplets can subsequently freeze, depending on the nature of the immersed aerosol particle and the adjusted temperature. At the LACIS outlet, a home-built optical particle spectrometer (*Clauss et al*., 2013) is used to determine if the arriving hydrometeors are liquid droples or frozen ice crystals. This information then is used to derive a frozen fraction, α.

Experimental uncertainties: The temperature uncertainty is $T \pm 0.3$K, the uncertainty of the measured α is on average ± 27.4%. The uncertainty in n_s was calculated accounting for this measurement uncertainty and for the uncertainty related to the width of the transfer function in the DMA, which was assumed to be 5%. The resulting uncertainty in n_s derived from LACIS data is 28%.

Meteorological Research Institute Dynamic Controlled Expansion Cloud-simulation Chamber (MRI-DCECC)

The DCECC at Meteorological Research Institute (MRI) in Tsukuba, Japan (*Tajiri et al.*, 2013) was used to investigate immersion freezing properties of dry illite NX particles. The DCECC can simulate quasi-adiabatic expansions by synchronously controlling air pressure and inner wall temperature of the chamber vessel. MRI-DCECC warrants experiments with atmospherically relevant droplet sizes as well as controllable droplet onset temperature ($T_{droplet,\ onset}$) and supersaturation conditions resulting in freezing of particles in water droplets. Dry illite NX particles were aerosolized by a rotating brush generator (PALAS, RBG1000) and injected into the ventilated 1.4 m^3 chamber vessel. All experiments were performed by employing a constant cooling rate of about -3 ˚C min^{-1} (equivalent to the updraft rate of about 5.0 m s^{-1}) from initial gas temperature typically about 5 ˚C. The DCECC is equipped with various devices, such as a SMPS, a welas-OPC, an APS and a CPC, for sensing cloud formation and measuring size distributions and shapes of aerosol and cloud particles from 0.01 to several hundred micrometers in size. As these instruments were also employed at AIDA-CECC, the procedures to calculate the total ice number and total geometric surface were also consistent with AIDA measurements.

Experimental uncertainties: The temperature uncertainty in MRI-DCECC is $T \pm 1.0$ °C for the evacuation rate corresponding to 5.0 m s^{-1}. The 40% uncertainty for n_s was derived from the errors in the measurements of N_{ice} by a welas (20%; *Möhler et al.*, 2006) and surface area estimation (34%). More specifically, the uncertainty for surface area estimation was derived from the relative standard deviation of the 10 s time-averaged welas surface measurements for approximately 5 min prior to expansion experiments (i.e., MRI02_131001a, MRI02_131003b and MRI02_131004).

Portable Ice Nucleation Chamber (PINC)

PINC operation principle is based on the Continuous Flow Diffusion Chamber (*Rogers*, 1988). Two flat parallel plates (568 x 300 mm) whose inner walls coated with ice before each experiment are temperature controlled so as to apply a temperature gradient between the ice layers leading to a supersaturation with respect to ice and water. This allows ice crystals to form and grow on ice nuclei in the water sub-saturated (RH_w < 100 %) and supersaturated (RH_w > 100 %) regimes thus inferring deposition and condensation freezing respectively. Any water drops that may form will evaporate in the evaporation section downstream of the freezing chamber. Upstream of PINC, aerosol particles are counted with a CPC after flowing through an impactor with a D_{50} cutoff at 0.91 µm aerodynamic diameter (*Chou et al*., 2011). The ice crystals are counted with an OPC at the exit of PINC and are distinguished from the small, unactivated aerosol particles by their size. For the data collected in this work, we counted all particles in size bins above 2 µm to be ice particles since the illite NX particles we sampled were 500 and 1000 nm in diameter. Measurements conducted for 3 min before each sample and one minute after a sample were averaged in order to determine the background signal in the OPC. These values were then subtracted from the IN concentrations obtained during sample measurement to correct for the background. Further details on the PINC design and operation are described in *Chou et al*. (2011) and *Kanji et al*. (2013).

Polydisperse illite NX particles that were suspended in the 4 m^3 volume aerosol buffer chamber were size-selected using a DMA and counted using a CPC after which they were sampled by PINC. The activated fraction is calculated by taking the ratio of the ice crystal number concentration to the total particle number concentration measured with the CPC. Particles with diameters 500 and 1000 nm were size-selected using the Maxi-DMA developed at the TROPOS and described in more detail elsewhere (*Raddatz et al*., 2013).

For comparison with other IN counters measuring in immersion mode, only IN data taken by PINC at $RH_w \geq 104$ % and below the RH_w at which droplets survive past the evaporation section ($RH_{w,ds}$), are presented. For each temperature, RH was scanned continuously from RH_{ice} = 100 % up to $RH_{w,ds}$. $RH_{w,ds}$ lies for T = -20 °C at 105 % and at -38 °C at 109 %.

Particle losses in the tubing and the impactor upstream of PINC were accounted for by a particle loss curve determined for kaolinite particles with a mobility diameter between 500 –

950 nm. As such the data for 500 and 1000 nm particles have been corrected for losses through the impactor of 25 and 60% respectively.

At lower temperatures, the results show reasonable agreement with AIDA and LACIS measurements, however at higher temperatures (-25 °C) we find that for the 1000 nm particle we underestimate the n_s compared to LACIS for example. The reason for this is that we do not have enough residence time in the growth and nucleation section of PINC (residence time of 4 – 5 s) to fully activate the particles into droplets and as such underestimate the AF in immersion mode. The way to compensate for this would be to sample at higher RH_w (as we do for lower temperatures), but at higher temperatures we are limited by the water drop survival line (RH_w = 105%) so we cannot compensate for the short residence time by taking data points at higher RH_w. As such, data taken for immersion freezing at higher temperatures could mean that we are underestimating immersion freezing, or rather be reporting deposition nucleation or condensation freezing.

Experimental uncertainties: Temperature uncertainties are on the order of ± 0.1 ˚C resulting in a relative uncertainty of ± 2% in *RH*. The temperature uncertainty results in a variation across the sample lamina of ± 0.4 ˚C. Uncertainty in N_{ice} (From OPC) is 10% and surface area estimate is about 25% resulting in an uncertainty in n_s of ± 27%.

PNNL Compact Ice Chamber (PNNL-CIC)

Heterogeneous ice nucleation properties of illite NX dust particles generated by the small-scale powder disc-disperser (SSPD, TSI, Model 3433) were investigated using ice nucleation chamber located at Atmospheric Measurement Laboratory, an atmospheric sciences laboratory at Pacific Northwest National Laboratory (PNNL), WA., USA. The working principle of PNNL compact ice chamber (PNNL-CIC) has been described in the literature (*Stetzer et al*., 2008; *Friedman et al*., 2011; *Kulkarni et al*., 2012); its design and experimental details are as follows. PNNL-CIC is a continuous flow diffusion chamber consisting of two flat, vertical parallel aluminum plates that are cooled and covered with a layer of ice. The chamber also has an evaporation section attached at the bottom of the chamber to remove water droplets. The chamber design ensures that aerosols are exposed to constant temperature and RH_{ice} over the length of the chamber. Saturation vapor pressures over ice and water are calculated using formulations published by *Murphy and Koop* (2005). The chamber wall temperatures are controlled by using two external cooling baths (Lauda Brinkmann Inc.), and temperature data are logged using the National Instrument CompactRIO programmable automation controller (cRIO-9114 combined with cRIO-9022). The chamber

plates are temperature controlled independently to develop a linear temperature gradient across them, which according to the principle of thermal gradient diffusion theory, produces a supersaturation profile between the plates (e.g., *Rogers et al*., 1988). Recently we modified the evaporation section design, such that this section now has separate cooling bath and its temperature is independently controlled. Temperature of the evaporation section is typically maintained at ~ −32 °C. At the beginning of the experiment, the chamber walls are coated with an ~ 0.5 mm thick ice layer, and the temperature gradient is set at zero, which creates ice-saturation conditions inside the chamber (RH_{ice} = 100 %), Then, the refrigeration system cools one plate and warms the other to increase the RH_{ice}. The total flow used is 11 L min^{-1}; sheath and sample flows used were 10 and 1 L min^{-1}, respectively, which limits the aerosol residence time to ~12 s within the CIC. Ice nucleates on the aerosol particles and the newly formed ice crystal grows to a size greater than the original aerosol size, and ice crystals >3 μm exiting the chamber are counted with an OPC (CLiMET, model CI-3100). The ice active fraction was calculated as the ratio of number of ice crystals measured by the OPC to the condensation nuclei available for nucleation. Background ice nuclei concentrations were calculated to estimate the lower detection limit of an α. The lower detection limit of α was <0.01 %. To make sure our background IN concentrations are less than 0.01 %, we restrict our experimental time to less than 3 hours.

Experimental uncertainties: Temperature uncertainty is ~± 0.3 ˚C. For n_s the uncertainty arises from N_{ice} measurement and surface area estimation. The resulting error is ~ ± one order of magnitude at any $n_s(T)$ space.

Zurich Ice Nucleation Chamber with Immersion Mode Cooling chAmber (IMCA-ZINC)

ZINC is a parallel plate CFDC type chamber developed by *Stetzer et al*. (2008) following the design described in the work of *Rogers* (1988). The chamber inner-walls are coated with ice prior to experiments. Under equilibrium conditions, linear temperature and vapor pressure gradients are established between the warmer and colder walls creating supersaturated conditions with respect to ice or water in the chamber volume. The two chamber walls are separately temperature-controlled by two cryostats (Lauda RP890). Independent temperature control of the two walls enables experiments at relative humidity conditions ranging from ice saturation until several hundred per cent of water saturation. An evaporation section, where both walls are kept at the same temperature to create ice saturated

but water-sub-saturated conditions, is able to evaporate potentially formed droplets, before being sampled by an OPC. Deposition mode experiments are conducted by scanning through relative humidity space while keeping the experimental temperature constant by increasing the temperature gradient between the two wall plates. The streamline of the injected illite NX particles (generated by a combination of a TSI fluidized bed, a series of URG cyclone impactors and a TSI DMA; *Welti et al*., 2009) is maintained at approximately the center position between the ice coated walls by two layers of particle-free sheath air. At the exit of ZINC, ice crystals are detected and distinguished from inactivated particles by size using an OPC (Climet Cl-3100). The particle concentration introduced into the experiment is detected with a butanol-CPC (TSI 3010).

The IMCA chamber was developed by *Lüönd et al*. (2010) as a vertical extension to ZINC and has the same parallel plate geometry. The walls are layered with continuously wetted filter papers and temperature controlled. Similar to ZINC, a horizontal temperature gradient is applied to create supersaturation with respect to water between the walls. When entering IMCA, particles are exposed to 120% saturation with respect to water at 40°C to trigger droplet formation and growth. Subsequently, a vertical temperature gradient is established to cool the formed droplets down to the experimental temperatures prevailing in ZINC. For immersion freezing experiments ZINC is held at water saturated conditions to prevent evaporation or droplet growth. Droplets and ice crystals are detected in line before entering ZINC's evaporation section using the Ice Optical Depolarization detector (IODE) described in *Nicolet et al*. (2010). IMCA-ZINC combination mimics an atmospheric pathway where particles are activated as cloud droplets at temperatures above 0°C, subsequently cooled and exposed to sub-zero temperatures at which freezing can occur.

Experimental uncertainties: Temperature uncertainty is ± 0.4 ˚C. The uncertainties in $n_s(T)$ are propagated from the uncertainties in IODE and the surface area (± 25%).

S2. Supplementary figures

X-ray diffraction measurement was performed by a Panalytical X`Pert Pro device (fixed divergence, 40 kV, 30 mA, $CuK_a$ exication). For data analysis the X`Pert Pro software was applied. While we successfully identify several different forms of orthoclase (KAlSi3O8) with some Na inclusion, we cannot specify the type of K-feldspar polymorphs (e.g., microcline). Therefore, we define the feldspar as presumably orthoclase or sanidine in the present study.

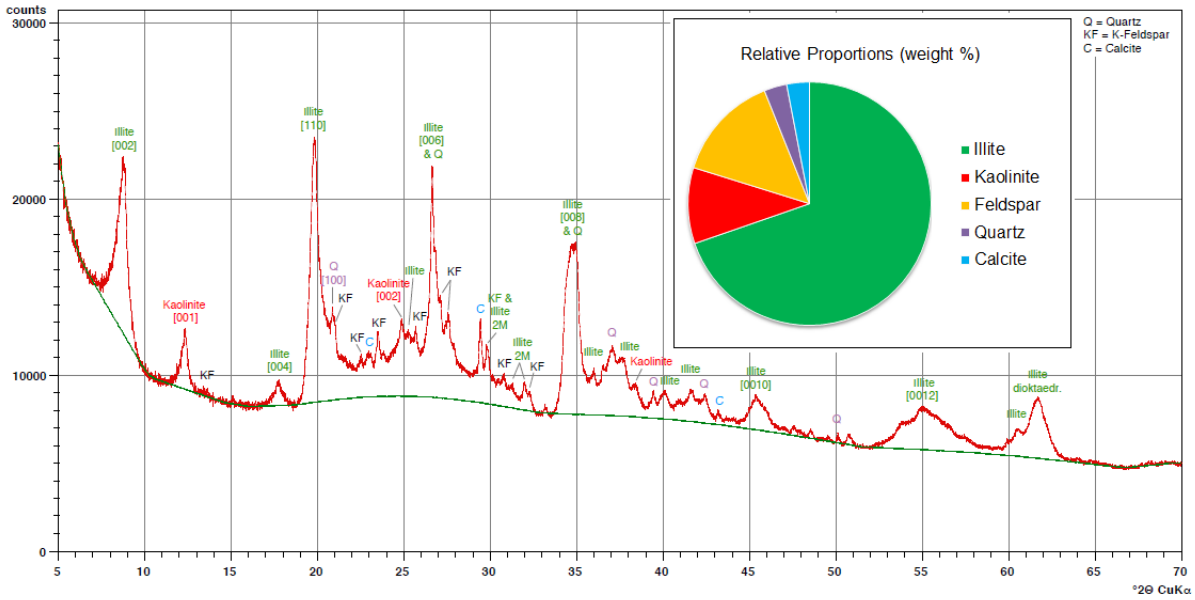

Figure S1. X-ray diffraction spectrum of the illite NX sample.

Spectra of $n_s(T)$ (Figs. 4 and 5) can be converted to $n_m(T)$ spectra using Eqn. 4. Illite NX insoluble and non-swelling dust, so $n_m(T)$ may not correctly represent its immersion freezing efficiency (*Murray et al.*, 2012). However, we note that this IN mass reflects the most direct representation of measurements with suspension since conversion of α into $n_{m,sus}(T)$ requires only one value, which is SSA (Eqn. 4).

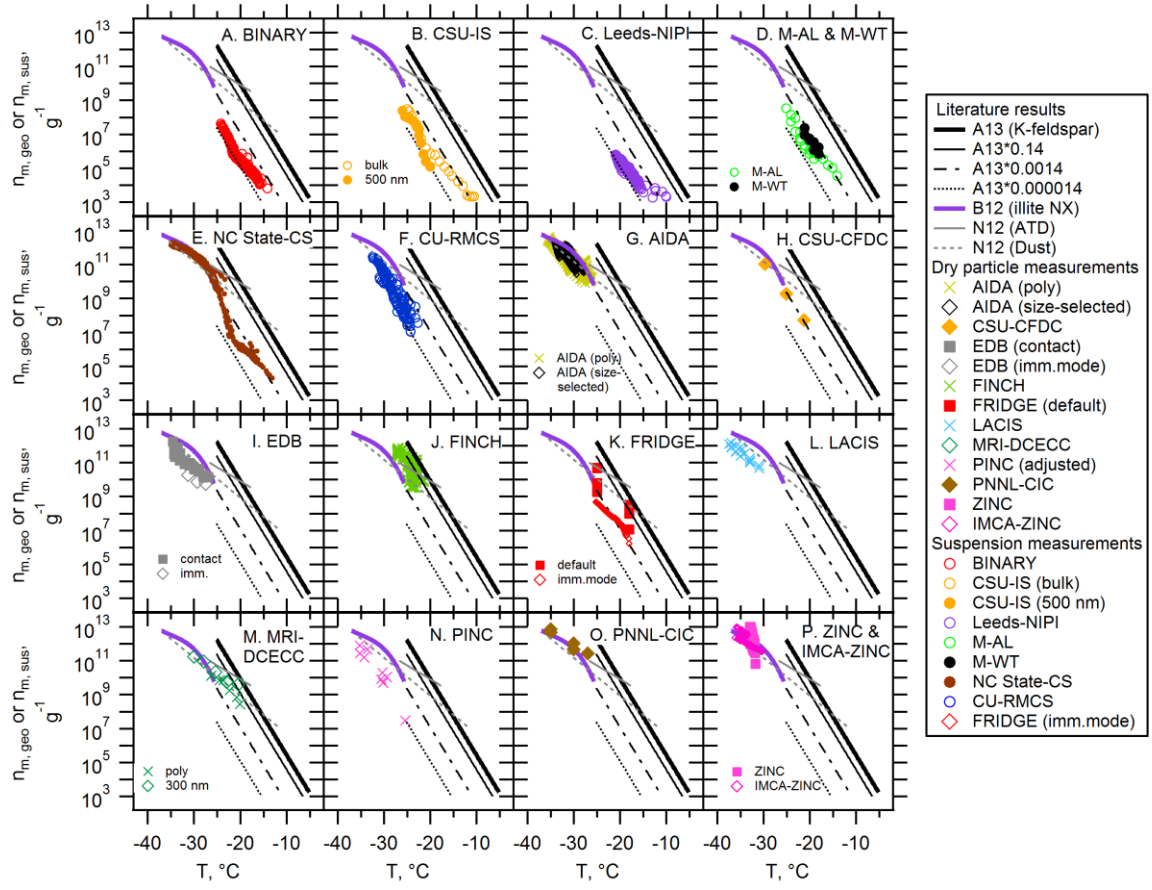

Figure S2. Inter-comparison of seventeen instruments with $n_{m,geo}$ or $n_{m,sus}$ (for dry-dispersed particle and suspension measurements, respectively). Note that M-AL and M-AT results are presented in single panel D.

S3. Supplementary table

A combination of four different methods for particle dispersion (rotating brush, flask dispersion, fluidized bed, or disc-dispersion method) and four types of DMA [commercially available one from TSI (Model 3081), Type Vienna Hauke medium (*Knutson and Whitby*, 1975) or custom built Maxi-DMA from TROPOS (*Raddatz et al*., 2013)] was employed for particle generation from illite NX samples. Further, most of the dry dispersion techniques used upstream impactors to filter out large agglomerated particles and safeguard against counting these large particles as INPs. Different types of dispersion method, impactor and size segregating instrument used in the present work are listed below.

Table S1. Summary of methods used for dry particle generation.

Instrument	Dispersion method	Size selecting instrument	Impactor type
AIDA*	Rotating brush	TSI DMA 3081	Cyclone impactors (D_{50} 1 μm and 5 μm)
CSU-CFDC	Flask dispersion	TSI DMA 3081	Dual single-jet impactors (cutpoint of 1.5 and 2.4 μm)
EDB*	Fluidized bed	TSI DMA 3081	Multistage impactor (cutpoint of 2 μm)
FINCH*	Fluidized bed	Type Vienna Hauke medium	MOUDI and cyclone impactors
FRIDGE*	Rotating brush	TSI DMA 3081	Cyclone impactor (D_{50} ~1.5 μm)
LACIS*	Fluidized bed	Type Vienna Hauke medium	MOUDI and cyclone impactors
MRI-DCECC	Rotating brush	TSI DMA 3081	Cyclone impactors (D_{50} of 2.5 μm and 1.0 μm)
PINC	Rotating brush	TROPOS Maxi-DMA	Impactor (D_{50} at 0.91 μm)
PNNL-CIC	Rotating disc dispersion	TSI DMA 3081	Cyclone impactor (D_{50} ~1 μm)
IMCA-ZINC	Fluidized bed	TSI DMA 3081	Cyclone impactors (D_{50} 3 μm and 1 μm)

*instruments of INUIT project partners.

S4. List of abbreviations, acronyms and symbols (alphabetical order)

AIDA:	Aerosol Interaction and Dynamics in the Atmosphere
APS:	aerodynamic particle sizer
ATD:	Arizona Test Dust
A13:	Atkinson's parameterization
BET:	Brunauer, Emmett, and Teller
BINARY:	Bielefeld Ice Nucleation ARraY
B12:	Broadley's parameterization
CEC:	Cation Exchange Capacity
CECC:	controlled expansion cloud-simulation chamber
CFDC:	continuous flow diffusion chamber
$c_{impurities}(T)$:	concentration of impurities per unit volume water at temperature T
$c_{IN}(T)$:	concentration of INP per unit volume water at temperature T
CNT:	classical nucleation theory
CPC:	condensation particle counter
CSU-IS:	Colorado State University Ice Spectrometer
CSU-CFDC:	Colorado State University Continuous Flow Diffusion Chamber
CU-RMCS:	University of Colorado Raman microscope cold stage
DCECC:	Dynamic Controlled Expansion Cloud-simulation Chamber
DfG:	German Research Society
DLS:	dynamic light scattering
DMA:	differential mobility analyzer
DSF:	dynamic shape factor
D:	average median diameter
D_{thresh}:	droplet-ice threshold diameter
D_{ve}:	volume equivalent midpoint diameter of individual particle
D_{50}:	cut size with a 50% mass of particles
D_{95}:	cut size with a 95% mass of particles
e_c:	probability of freezing on a single contact
EDB:	ElectroDynamic Balance
EDX:	energy dispersive X-ray
FINCH:	Fast Ice Nucleus CHamber
FRIDGE:	FRankfurt Ice Deposition freezinG Experiment
f:	proportion of droplets not frozen
f_{ice}:	frozen fraction after time t
f^*_{ice}:	fraction of droplets frozen
$f_{unfrozen}$:	fraction of unfrozen drops at each particular temperature
$Hor_{Max\text{-}Min}$:	horizontal T deviation between maxima and minima in $n_s(T)$ spectrum
IC:	ion chromatography
ICIS-2007:	international ice nucleation workshop in 2007
illite NX:	commercially available NX Nanopowder illite-rich dust from Arginotec
IMCA-ZINC:	Zurich Ice Nucleation Chamber with Immersion Mode Cooling-chAmber
IN	ice nucleation
INP:	ice nucleating particle
INUIT:	Ice Nucleation research UnIT
J_{imm}:	immersion freezing rate coefficient
K-feldspar:	potassium-rich feldspar

$K'(T)$: cumulative INP concentration at a temperature T
LACIS: Leipzig Aerosol Cloud Interaction Simulator
Leeds-NIPI: Leeds Nucleation by Immersed Particles Instrument
M-AL: Mainz Acoustic Levitator
M-WT: Mainz vertical Wind Tunnel
min: minute
MRI-DCECC: Meteorological Research Institute DCECC
M_{total}: total mass
M_{ve}: volume equivalent mass of individual particle
n_c: collision rate
NC State-CS: North Carolina State cold stage
N_{ae}: number of aerosols
$N_{droplet}$: number of droplets
N_{ice}: number concentration of ice crystals
$n_{m,geo}$: geometric mass-based ice nucleating mass
$n_{m,sus}$: ice nucleating mass derived from suspension measurements
n_s: IN active surface-site density
$n_{s,BET}$: BET surface-inferred n_s
$n_{s,geo:}$ geometric size based n_s
$N(T)$: number of frozen droplets at temperature T
N_{total}: total number concentration of particles
N_0: total number of droplets
N12: Niemand's parameterization
OPC: optical particle counter
OPS: optical particle sizer
PCR: polymerase chain reaction
PDF: probability density function
PDMS: polydimethylsiloxane
PINC: Portable Ice Nucleation Chamber
PNNL-CIC: Pacific Northwest National Laboratory Compact Ice Chamber
r: correlation coefficient
RH_{ice}: relative humidity with respect to ice
RH_w: relative humidity with respect to water
$RH_{w,ds}$: RH_w at which droplets survive past the evaporation section
s: second
SBM: soccer ball model
SIMONE: Streulicht-intensitätsmessungen zum optischen Nachweis von Eispartikeln
S_{IN}: surface area of a single ice nucleating particle
SMPS: scanning mobility particle sizer
SSA: specific surface area
S_{total}: total surface area
S_{ve}: volume equivalent surface area of individual particle
t: time
T: temperature
TDL: tunable diode laser
$T_{droplet,\ onset}$: droplet onset temperature
TROPOS: Leibniz Institute for Tropospheric Research
UHSAS: Ultra-High Sensitivity Aerosol Spectrometer
V: droplet volume
V_{drop}: median drop volume of the population
$Ver_{Max\text{-}Min}$: vertical n_s deviation between maxima and minima in $n_s(T)$ spectrum

818	w:	mass ratio of dust and water (g dust/g water)
819	wt%:	weight percent
820	x:	volume of water used to wash the particles from the filter
821	XRD:	X-ray diffraction
822	y:	volume of air sampled through the filter
823	α:	ice activated fraction (= N_{ice}/N_{total})
824	θ:	specific surface area measured by BET technique
825	θ_{N2}:	specific surface area measured by BET technique with nitrogen gas
826	θ_{H2O}:	specific surface area measured by BET technique with water vapor
827	ρ:	particle density of illite NX
828	ρ_w:	density of water (0.9971 g H_2O/m^3 H_2O)
829	χ:	dynamic shape factor

References

Agresti, A. and Coull, B. A.: Approximate is better than "exact" for interval estimation of binomial proportions. Am. Stat., 52, 119–126, doi:10.2307/2685469, 1998.

Ardon-Dryer, K. and Levin, Z.: Ground-based measurements of immersion freezing in the eastern Mediterranean, Atmos. Chem. Phys., 14, 5217–5231, doi:10.5194/acp-14-5217-2014, 2014.

Atkinson, J. D., Murray, B. J., Woodhouse, M. T., Carslaw, K., Whale, T. F., Baustian, K., Dobbie, S., O'Sullivan, D., and Malkin, T. L.: Nature, 498, 355–358, doi:10.1038/nature12278, 2013.

Baustian, K. J., Wise, M. E., and Tolbert, M. A.: Depositional ice nucleation on solid ammonium sulfate and glutaric acid particles, Atmos. Chem. Phys., 10, 2307–2317, doi:10.5194/acp-10-2307-2010, 2010.

Benz, S., Megahed, K., Möhler, O., Saathoff, H., Wagner, R., and Schurath, U.: T-dependent rate measurements of homogeneous ice nucleation in cloud droplets using a large atmospheric simulation chamber, J. Photoch. Photobio. A, 176, 208–217, doi:10.1016/j.jphotochem.2005.08.026, 2005.

Broadley, S. L., Murray, B. J., Herbert, R. J., Atkinson, J. D., Dobbie, S., Malkin, T. L., Condliffe, E., and Neve, L.: Immersion mode heterogeneous ice nucleation by an illite rich powder representative of atmospheric mineral dust, Atmos. Chem. Phys., 12, 287–307, doi:10.5194/acp-12-287-2012, 2012.

Budke, C. and Koop, T.: BINARY : An Optical Freezing Array for Assessing Temperature and Time Dependence of Heterogeneous Ice Nucleation, Atmos. Meas. Tech. Discuss., 7, accepted, 2014.

Bundke, U., Nillius, B., Jaenicke, R., Wetter, T., Klein, H., and Bingemer, H.: The fast ice nucleus chamber FINCH, Atmos. Res., 90, 180–186, doi:10.1016/j.atmosres.2008.02.008, 2008.

Bundke, U., Reimann, B., Nillius, B., Jaenicke, R., and Bingemer, H.: Development of a Bioaerosol single particle detector (BIO IN) for the Fast Ice Nucleus CHamber FINCH, Atmos. Meas. Tech., 3, 263–271, doi:10.5194/amt-3-263-2010, 2010.

Chou, C., Stetzer, O.,Weingartner, E., Jurányi, Z., Kanji, Z. A., and Lohmann, U.: Ice nuclei properties within a Saharan dust event at the Jungfraujoch in the Swiss Alps, Atmos. Chem. Phys., 11, 4725–4738, doi:10.5194/acp-11-4725-2011, 2011.

Clauss, T., Kiselev, A., Hartmann, S., Augustin, S., Pfeifer, S., Niedermeier, D., Wex, H., and Stratmann, F.: Application of linear polarized light for the discrimination of frozen and liquid droplets in ice nucleation experiments, Atmos. Meas. Tech., 6, 1041–1052, doi:10.5194/amt-6-1041-2013, 2013.

878 DeMott, P. J. and Coauthors: Resurgence in ice nuclei measurement research, B. Am.
879 Meteorol. Soc., 92, 1623–1635, doi:http://dx.doi.org/10.1175/2011BAMS3119.1, 2011.
880
881 DeMott, P. J., Prenni, A. J., McMeeking, G. R., Sullivan, R. C., Petters, M. D., Tobo, Y.,
882 Niemand, M., Möhler, O., Snider, J. R., Wang, Z., and Kreidenweis, S. M.: Integrating
883 laboratory and field data to quantify the immersion freezing ice nucleation activity of mineral
884 dust particles, Atmos. Chem. Phys. Discuss., 14, 17359–17400, doi:10.5194/acpd-14-17359-
885 2014, 2014.
886
887 Diehl, K., Mitra, S. K., Szakáll, M., Blohn, N. v., Borrmann, S., and Pruppacher, H.R.:
888 Chapter 2. Wind tunnels: Aerodynamics, models, and experiments. In: The Mainz vertical
889 wind tunnel facility: A review of 25 years of laboratory experiments on cloud physics and
890 chemistry [Pereira, J. D. (eds.)], Nova Science Publishers, Inc., 2011.
891
892 Diehl, K., Debertshäuser, M., Eppers, O., Schmithüsen, H., Mitra, S.K., and Borrmann, S.:
893 Particle-area dependence of mineral dust in the immersion mode; investigations with freely
894 suspended drops in an acoustic levitator. Atmos. Chem. Phys. Discuss., 14, 12887–12930,
895 doi:10.5194/acpd-14-12887-2014, 2014.
896
897 Eidhammer, T., DeMott, P. J., Prenni, A. J., Petters, M. D., Twohy, C. H., Rogers, D. C.,
898 Stith, J., Heymsfield, A., Wang, Z., Haimov, S., French, J., Pratt, K., Prather, K., Murphy, S.,
899 Seinfeld, J., Subramanian, R., and Kreidenweis, S. M.: Ice initiation by aerosol particles:
900 Measured and predicted ice nuclei concentrations versus measured ice crystal concentrations
901 in an orographic wave cloud. J. Atmos. Sci., 67, 2417–2436. doi: 10.1175/2010JAS3266.1,
902 2010.
903
904 Fahey, D. W., Gao, R.-S., Möhler, O., Saathoff, H., Schiller, C., Ebert, V., Krämer, M., Peter,
905 T., Amarouche, N., Avallone, L. M., Bauer, R., Bozóki, Z., Christensen, L. E., Davis, S. M.,
906 Durry, G., Dyroff, C., Herman, R. L., Hunsmann, S., Khaykin, S. M., Mackrodt, P., Meyer, J.,
907 Smith, J. B., Spelten, N., Troy, R. F., Vömel, H., Wagner, S., and Wienhold, F. G.: The
908 AquaVIT-1 intercomparison of atmospheric water vapor measurement techniques, Atmos.
909 Meas. Tech. Discuss., 7, 3159–3251, doi:10.5194/amtd-7-3159-2014, 2014.
910
911 Friedman, B., Kulkarni, G., Beránek, J., Zelenyuk, A., Thornton, J. A., and Cziczo, D. J.: Ice
912 nucleation and droplet formation by bare and coated soot particles, J. Geophys. Res., 116,
913 D17203, doi:10.1029/2011JD015999, 2011.
914
915 Hader, J. D., Wright, T. P., and Petters, M. D.: Contribution of pollen to atmospheric ice
916 nuclei concentrations, Atmos. Chem. Phys., 14, 5433–5449, doi:10.5194/acp-14-5433-2014,
917 2014.
918
919 Hartmann, S., Niedermeier, D., Voigtländer, J., Clauss, T., Shaw, R. A., Wex, H., Kiselev, A.,
920 and Stratmann, F.: Homogeneous and heterogeneous ice nucleation at LACIS: operating
921 principle and theoretical studies, Atmos. Chem. Phys., 11, 1753–1767, doi:10.5194/acp-11-
922 1753-2011, 2011.
923
924 Herbert, R. J., Murray, B. J., Whale, T. F., Dobbie, S. J., and Atkinson, J. D.: Representing
925 time-dependent freezing behaviour in immersion mode ice nucleation, Atmos. Chem. Phys.,
926 14, 8501-8520, doi:10.5194/acp-14-8501-2014, 2014.
927

928 Hiranuma, N., Paukert, M., Steinke, I., Zhang, K., Kulkarni, G., Hoose, C., Schnaiter, M.,
929 Saathoff, H., and Möhler, O.: A comprehensive parameterization of heterogeneous ice
930 nucleation of dust surrogate: laboratory study with hematite particles and its application to
931 atmospheric models, Atmos. Chem. Phys. Discuss., 14, 16493–16528, doi:10.5194/acpd-14-
932 16493-2014, 2014a.
933
934 Hiranuma, N., Hoffmann, N., Kiselev, A., Dreyer, A., Zhang, K., Kulkarni, G., Koop, T., and
935 Möhler, O.: Influence of surface morphology on the immersion mode ice nucleation
936 efficiency of hematite particles, Atmos. Chem. Phys., 14, 2315–2324, doi:10.5194/acp-14-
937 2315-2014, 2014b.
938
939 Hoffmann, N., Duft, D., Kiselev, A., and Leisner, T.: Contact freezing efficiency of mineral
940 dust aerosols studied in an electrodynamic balance: quantitative size and temperature
941 dependence for illite particles, Faraday Discuss., 165, 383–390, doi:10.1039/C3FD00033H,
942 2013a.
943
944 Hoffmann, N., Kiselev, A., Rzesanke, D., Duft, D., and Leisner, T.: Experimental
945 quantification of contact freezing in an electrodynamic balance, Atmos. Meas. Tech., 6, 2373–
946 2382, doi:10.5194/amt-6-2373-2013, 2013b.
947
948 Hu, Y.-X., Yang, P., Lin, B., Gibson, G., Hostetler, C.: Discriminating between spherical and
949 non-spherical scatterers with lidar using circular polarization: a theoretical study. J. Quant.
950 Spectrosc. Radiat. Transfer 79–80, 757–764, doi:10.1016/S0022-4073(02)00320-5, 2003.
951
952 Kanji, Z. A., Welti, A., Chou, C., Stetzer, O., and Lohmann, U.: Laboratory studies of
953 immersion and deposition mode ice nucleation of ozone aged mineral dust particles, Atmos.
954 Chem. Phys., 13, 9097–9118, doi:10.5194/acp-13-9097-2013, 2013.
955
956 Klein, H., Haunold, W., Bundke, U., Nillius, B., Wetter, T., Schallenberg, S., and Bingemer,
957 H.: A new method for sampling of atmospheric ice nuclei with subsequent analysis in a static
958 diffusion chamber, Atmos. Res., 96, 218–224, doi:10.1016/j.atmosres.2009.08.002, 2010.
959
960 Knutson, E. O., and Whitby, K. T.: Aerosol classification by electric mobility: apparatus,
961 theory, and applications. Aerosol Sci., 6, 6, 443–451, doi:10.1016/0021-8502(75)90060-9,
962 1975.
963
964 Kulkarni, G., Fan, J., Comstock, J. M., Liu, X., and Ovchinnikov, M.: Laboratory
965 measurements and model sensitivity studies of dust deposition ice nucleation, Atmos. Chem.
966 Phys., 12, 7295–7308, doi:10.5194/acp-12-7295-2012, 2012.
967
968 Langham, E. J. and Mason, B. J.: The heterogeneous and homogeneous nucleation of
969 supercooled water. Proceedings of the Royal Society A: Mathematical, Physical and
970 Engineering Sciences, 247, 1251, 493–504. doi:10.1098/rspa.1958.0207, 1958.
971
972 Lüönd, F., Stetzer, O., Welti, A., and Lohmann, U.: Experimental study on the ice nucleation
973 ability of size-selected kaolinite particles in the immersion mode, J. Geophys. Res., 115,
974 D14201, doi:10.1029/2009JD012959, 2010.
975
976 Möhler, O., Stetzer, O., Schaefers, S., Linke, C., Schnaiter, M., Tiede, R., Saathoff, H.,
977 Krämer, M., Mangold, A., Budz, P., Zink, P., Schreiner, J., Mauersberger, K., Haag, W.,
978 Kärcher, B., and Schurath, U.: Experimental investigation of homogeneous freezing of

sulphuric acid particles in the aerosol chamber AIDA, Atmos. Chem. Phys., 3, 211–223, doi:10.5194/acp-3-211-2003, 2003.

Möhler, O., Field, P. R., Connolly, P., Benz, S., Saathoff, H., Schnaiter, M., Wagner, R., Cotton, R., Krämer, M., Mangold, A., and Heymsfield, A. J.: Efficiency of the deposition mode ice nucleation on mineral dust particles, Atmos. Chem. Phys., 6, 3007–3021, doi:10.5194/acp-6-3007-2006, 2006.

Murphy, D. M., and Koop, T.: Review of the vapour pressures of ice and supercooled water for atmospheric applications, Q. J. R. Meteorol. Soc., 131, 1539–1565, doi:10.1256/qj.04.94, 2005.

Murray, B. J., Broadley, S. L., Wilson, T. W., Atkinson, J. D., and Wills, R. H.: Heterogeneous freezing of water droplets containing kaolinite particles, Atmos. Chem. Phys., 11, 4191–4207, doi:10.5194/acp-11-4191-2011, 2011.

Murray, B. J., O'Sullivan, D., Atkinson, J. D., and Webb, M. E.: Ice nucleation by particles immersed in supercooled cloud droplets, Chem. Soc. Rev., 41, 6519–6554, doi:10.1039/c2cs35200a, 2012.

Nicolet, M., Stetzer, O., Lüönd, F., Möhler, O., and Lohmann, U.: Single ice crystal measurements during nucleation experiments with the depolarization detector IODE, Atmos. Chem. Phys., 10, 313–325, doi:10.5194/acp-10-313-2010, 2010.

O'Sullivan, D., Murray, B. J., Malkin, T. L., Whale, T. F., Umo, N. S., Atkinson, J. D., Price, H. C., Baustian, K. J., Browse, J., and Webb, M. E.: Ice nucleation by fertile soil dusts: relative importance of mineral and biogenic components, Atmos. Chem. Phys., 14, 1853–1867, doi:10.5194/acp-14-1853-2014, 2014.

Petters, M. D., Parsons, M. T., Prenni, A. J., DeMott, P. J., Kreidenweis, S. M., Carrico, C. M., Sullivan, A. P., McMeeking, G. R., Levin, E., Wold, C. E., Collett, J. L. Jr., and Moosmüller, H.: Ice nuclei emissions from biomass burning, J. Geophys. Res., 114, D07209, doi:10.1029/2008JD011532, 2009.

Prenni, A. J., DeMott, P. J., Rogers, D. C., Kreidenweis, S. M., McFarquhar, G. M., Zhang, G., and Poellot, M. R.: Ice nuclei characteristics from M-PACE and their relation to ice formation in clouds, Tellus, 61B, doi:10.1111/j.1600-0889.2009.00415.x, 436-448. 2009.

Raddatz, M., Wiedensohler, A., Wex, H., and Stratmann, F.: Size selection of sub- and super-micron clay mineral kaolinite particles using a custom-built Maxi-DMA, AIP Conference Proceedings, 1527, 457–460, 2013.

Richardson, M.: Making real time measurements of ice nuclei concentrations at upper tropospheric temperatures: Extending the capabilities of the continuous flow diffusion chamber, DISSERTATION thesis, Colorado State Univ., Fort Collins, CO, USA, 268 pp, 2009.

Rzesanke, D., Nadolny, J., Duft, D., Muller, R., Kiselev, A., and Leisner, T.: On the role of surface charges for homogeneous freezing of supercooled water microdroplets, Phys. Chem. Chem. Phys., 14, 9359–9363, doi:10.1039/c2cp23653b, 2012.

Rogers, D. C.: Development of a continuous flow thermal gradient diffusion chamber for ice nucleation studies, Atmos. Res., 22, 149–181, doi:10.1016/0169-8095(88)90005-1, 1988.

Rogers, D. C., DeMott, P. J., Kreidenweis, S. M., and Chen, Y.: A continuous-flow diffusion chamber for airborne measurements of ice nuclei, J. Atmos. Oceanic Technol., 18, 725–741, doi:http://dx.doi.org/10.1175/1520-0426(2001)018<0725:ACFDCF>2.0.CO;2, 2001.

Schill, G. P. and Tolbert, M. A.: Heterogeneous ice nucleation on phase-separated organic-sulfate particles: effect of liquid vs. glassy coatings, Atmos. Chem. Phys., 13, 4681–4695, doi:10.5194/acp-13-4681-2013, 2013.

Schnaiter, M., Büttner, S., Möhler, O., Skrotzki, J., Vragel, M., and Wagner, R.: Influence of particle size and shape on the backscattering linear depolarisation ratio of small ice crystals – cloud chamber measurements in the context of contrail and cirrus microphysics, Atmos. Chem. Phys., 12, 10465-10484, doi:10.5194/acp-12-10465-2012, 2012.

Steinke, I., Möhler, O., Kiselev, A., Niemand, M., Saathoff, H., Schnaiter, M., Skrotzki, J., Hoose, C., and Leisner, T.: Ice nucleation properties of fine ash particles from the Eyjafjallajökull eruption in April 2010, Atmos. Chem. Phys., 11, 12945–12958, doi:10.5194/acp-11-12945-2011, 2011.

Stetzer, O., Baschek, B., Luond, F., and Lohmann, U.: The Zurich Ice Nucleation Chamber (ZINC) – A new instrument to investigate atmospheric ice formation, Aerosol Sci. Technol., 42, 64–74, doi:10.1080/02786820701787944, 2008.

Sullivan, R. C., Petters, M. D., DeMott, P. J., Kreidenweis, S. M., Wex, H., Niedermeier, D., Hartmann, S., Clauss, T., Stratmann, F., Reitz, P., Schneider, J., and Sierau, B.: Irreversible loss of ice nucleation active sites in mineral dust particles caused by sulphuric acid condensation, Atmos. Chem. Phys., 10, 11471–11487, doi:10.5194/acp-10-11471-2010, 2010a.

Sullivan, R. C., Miñambres, L., DeMott, P. J., Prenni, A. J., Carrico, C. M., Levin, E. J. T., and Kreidenweis, S. M.: Chemical processing does not always impair heterogeneous ice nucleation of mineral dust particles, Geophys. Res. Lett., 37, L24805, doi:10.1029/2010GL045540, 2010b.

Szakáll, M., Diehl, K., Mitra, S. K., and Borrmann, S.: A wind tunnel study on the shape, oscillation, and internal circulation of large raindrops with sizes between 2.5 and 7.5 mm, J. Atmos. Sci., 66, 755–765, doi:http://dx.doi.org/10.1175/2008JAS2777.1, 2009.

Tajiri, T., Yamashita, K., Murakami, M., Orikasa, N., Saito, A., Kusunoki, K., and Lilie, L.: A novel adiabatic-expansion-type cloud simulation chamber. J. Meteor. Soc. Japan, 91, 5, 687–704, doi:http://dx.doi.org/10.2151/jmsj.2013-509, 2013.

Tobo, Y., DeMott, P. J., Hill, T. C. J., Prenni, A. J., Swoboda-Colberg, N. G., Franc, G. D., and Kreidenweis, S. M.: Organic matter matters for ice nuclei of agricultural soil origin, Atmos. Chem. Phys. Discuss., 14, 9705–9728, doi:10.5194/acpd-14-9705-2014, 2014.

Vali, G.: Quantitative evaluation of experimental results an the heterogeneous freezing nucleation of supercooled liquids. J. Atmos. Sci., 28, 402–409. doi:http://dx.doi.org/10.1175/1520-0469(1971)028<0402:QEOERA>2.0.CO;2, 1971.

Wex, H., DeMott, P. J., Tobo, Y., Hartmann, S., Rösch, M., Clauss, T., Tomsche, L., Niedermeier, D., and Stratmann, F.: Kaolinite particles as ice nuclei: learning from the use of different kaolinite samples and different coatings, Atmos. Chem. Phys., 14, 5529–5546, doi:10.5194/acp-14-5529-2014, 2014.

Wright, T. P. and Petters, M. D.: The role of time in heterogeneous freezing nucleation, J. Geophys. Res. Atmos., 118, 3731–3743, doi:10.1002/jgrd.50365, 2013.